Numerical Methods in Civil Engineering

Journal Homepage: https://nmce.kntu.ac.ir/

Application of Artificial Neural Networks for Developing Temperature-Dependent Fragility Curves for Vulnerability Assessment of I-Girder Bridges

Saeid Sabouri Ghomi[*], Saman Shiravand[**], Mohammad Mahdi Zare Zardeyni[***], Najib Rabiee[****]

ARTICLE INFO

RESEARCH PAPER

Article history:
Received:
February 2025
Revised:
March 2025
Accepted:
April 2025

Keywords:
multi-hazard, post-fire seismic performance, artificial neural networks, steel I-girder bridges, high temperatures, grid search

Abstract

Although previous investigations have shown that a bridge's overall capacity may remain largely intact after a fire, its seismic performance in the aftermath of such events remains poorly understood. The primary objective of this study is to investigate the influence of fire on the seismic performance of a multi-span simply supported steel I-girder (MSSSS-IG). To achieve this, an artificial neural network (ANN) model was used to develop a multivariate probabilistic seismic demand model (MPSDM) and fragility curve. A total of 1,600 three-dimensional MSSSS-IG bridge models were generated using the OpenSees tool, incorporating material and geometric variability through Latin Hypercube Sampling (LHS). A set of 1,600 ISO 834 fires featuring peak temperatures varying between 200 °C to 1,000 °C was developed. The maximum temperature in the column was determined through heat transfer analysis. Accordingly, column reduction factors were computed via Eurocode provisions. Bridge, reduction factors, and input ground motion records were randomly paired using nonlinear response history analysis (NRHA). The XGBoost technique and grid search were employed to identify the important features and calibration hyperparameters of ANNs, respectively. It can be pointed out that the proposed ANN algorithm accurately estimates the component demands. Moreover, fragility findings demonstrate that local fire exposure in the column, ranging from 12.30 % and 22.30 %, increases the probability of system-level bridge failure.

1. Introduction

Growing demand for ground transportation and rapid urbanization have made the impact of fire on bridges an increasingly critical concern [1]. Data gathered from 1746 bridges that sustained damage in the United States between 1960 and 2013 reveal that fire was 2.7 times more detrimental than earthquake in bridges [2]. A similar study confirmed that, while earthquakes destroyed 1.8% of bridges in the United States between 1980 and 2012, fire caused damage to 2.1% of them [3]. Although several cases have demonstrated the detrimental effects of fire on bridge performance, there are no guidelines or recommendations for designing and assessing bridges under fire threats, unlike those available for buildings and tunnels [4-7].

Furthermore, due to the high cost, environmental issues, and capability protection threats connected with full-scale fire testing, numerical modeling continues to be the principal approach for assessing the performance of bridges subjected to fire [8].

The influence of fire on the performance of steel bridges indicates that a blaze occurring beneath the mid-span is less severe than one near the abutment [9]. Cui and Chen [8] proposed a simplified framework to account for the effects of wind and vehicle-induced fire, concluding that wind significantly intensifies the burning phase on the bridge deck. They also found that flame temperature and tilt angle may be affected, with increased wind speed causing a decrease in temperature and an increase in tilt angle. Zhang et al. [10] highlight that various parameters influence the resistance of horizontally curved bridges. Bridge behavior can be affected by multiple hazards throughout its service

[*] *Professor, Department of Civil and Environmental Engineering, K.N. Toosi University of Technology, Tehran, Iran. Email: sabouri@kntu.ac.ir*
[**] *PhD candidate, Department of Civil and Environmental Engineering, K.N. Toosi University of Technology, Tehran, Iran. Email: samanshiravand@email.kntu.ac.ir*
[***] *MSc student, Department of Civil and Environmental Engineering, K.N. Toosi University of Technology, Tehran, Iran. Email: mmahdi.zare95@gmail.com*
[****] *corresponding author, MSc student, Department of Civil and Environmental Engineering, K.N. Toosi University of Technology, Tehran, Iran Email: n.rabiee@email.kntu.ac.ir*

https://doi.org/10.61186/NMCE.2504.1087

life, including earthquakes and fires [11]. Fire can occur before and after an earthquake; the same researcher studies the effects of fire following earthquakes in buildings [12], [13], and some others look at the impact of earthquakes following a fire in structures [14]. In contrast, the combined effect of fire and earthquake hazards on bridges has received little attention to date.

Machine learning (ML) is an artificial intelligence branch that aims to learn from data, find patterns, or cluster data sets. Several investigations have explored the application of ML algorithms to bridges subjected to various hazards and environmental conditions. The suggested framework, which relies on the support vector regression (SVR) model, demonstrates that traffic loads may significantly enhance fatigue damage in suspended bridge hangers [15]. The ANN model, used to predict deterioration in concrete bridge decks, indicates that the deck's age, area, average daily traffic, and skew angle are significant features for predicting the response [16]. Regarding changing regional temperatures, the AANs model, which was trained based on the backpropagation method, highlights the vulnerability of LRB-isolated bridge components and system levels based on generated fragility curves, especially in the extensive and complete damage stages [17].

To predict the temperature in a flat box steel girder bridge, the proposed model, which was developed based on a hybrid random forest (RF) and Bayesian optimization, surged approximately 60% in prediction performance compared to the linear regression (LR) model [18]. In a similar study, an ANN framework was developed to predict bridge temperatures based on air temperatures [19]. Different ML models, including RF and Support Vector Machine (SVM), were investigated to classify the steel and concrete bridges under fire risk [20]. The results indicate that RF showed promising performance in detecting various degrees of fire-induced damage. Under simultaneous impacts of fire and corrosion, the appropriate least square SVM algorithm was demonstrated [21].

Although several studies have been implemented to better understand the influence of fire on the behavior of bridges [9-11], the results of previous investigations have shown that fire causes the collapse only around 4% of bridges [1-2]. Similarly, the estimated residual strength of a steel girder bridge under fire, evaluated at room temperature and different temperatures, showed that at 600 °C and 800 °C, respectively, 84% and 70% of the bridge's capacity remained [22]. As a result, estimating the remaining post-fire seismic capacity of bridges is crucial. This importance arises from the substantial residual capacity that bridges often retain after fire exposure[22], as well as the relatively low probability of collapse during fire events [1-2]. However, the studies that investigated the impact of fire following earthquakes on the seismic performance of bridges are limited.

In this field, Rabiee et al. explored the effect of fire on the seismic performance of bridges [1]. However, their study was limited by the use of a linear model to represent the demand model, did not account for uncertainty, and only investigated fire effects at a specific intensity level. Therefore, this study proposes an ANN-based framework to overcome the limitations of previous research by investigating the impact of local fire on the seismic performance of bridges across a wide range of fire intensities, while accounting for both epistemic and aleatory uncertainties.

First, 1,600 MSSSS-IG bridges, incorporating various sources of uncertainty, are modeled using the OpenSees platform. Each bridge sample is randomly paired with 160 input ground motion records, scaled at 20 different intensity levels ranging from 0.10 g to 2.0 g, and NRHAs are performed. In total, 64,000 NRHAs are conducted to train the ANN algorithm. Seventy percent of the datasets is used for training the ANN, while the remaining 30% is reserved for testing. Second, to maximize accuracy, grid search is employed to optimize the hyperparameters of the ANN models.

Third, seismic demand models are developed for a wide range of bridge components by incorporating 42 uncertainty parameters. Fourth, the XGBoost algorithm is employed to conduct a sensitivity analysis and identify the most influential bridge features. Fifth, grid search is again used to fine-tune the ANN hyperparameters, this time using only the significant features identified through XGBoost. Sixth, demand models for bridge components are developed based on these selected features, and their performance is compared with that of classical linear Finally, fragility curves at both component and system levels are generated to evaluate the influence of local fire on the seismic performance of bridges.

The remainder of the paper is organized as follows: Section 2 describes the prototype of the bridge and its computational modeling. Section 3 presents the input motion used for implementing NRHAs. The fire simulation, the methodology for applying fire, and associated fire scenarios are discussed in Section 4. Section 5 describes the ML model, feature selection, and assessment metric. Section 6 discusses the preprocessing approach, which includes presenting the method of generating the dataset and defining input and output variables. Finally, in Section 7, the results obtained for the ANN model are presented and discussed.

2. Bridge description

The first step in establishing the demand model involves grouping bridge types with similar performance during an

earthquake [23]. In the study, 1600 MSSSS-IG bridges were taken into consideration to develop the post-fire demand model. These bridges were built post-1990 seismic era, adhering to higher seismic criteria than older bridges. The number of columns per bent varied between one to three in seat abutments [24]. MSSSS-IG bridges with identical approach lengths and a central span length ratio of 0.4 are illustrated in Figure 1. More details about the design of MSSSS-IG bridges are explained in Figure 2 and Table 1.

LHS was used to account for a wide range of uncertainties in bridge modeling. This method ensures that all combinations of the uncertain parameters are considered in the modeling process, thereby providing more accurate simulations. It also allows for efficient use of computational resources, as fewer model runs are needed to capture the bridge response. Uncertainties related to structural geometry and material properties are summarized in Table 2 [25].

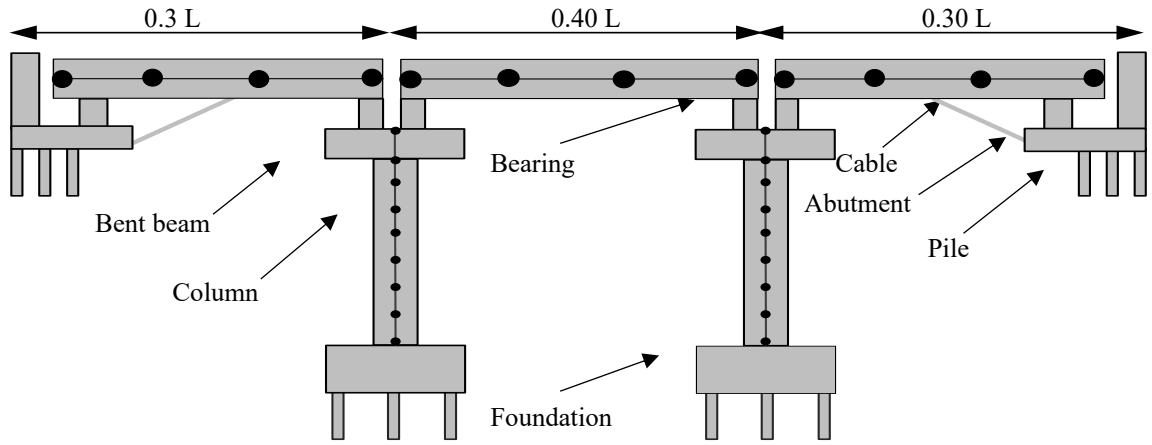

Fig. 1: Diagram illustrating a typical prototype bridge.

Table 1: Bridge specifications for different widths.

Width (m)	Number of columns per bent	Number of girders	Cover of the deck (m)	Slab thickness (m)
10.00< W<10.76	1	5	0.975	0.178
10.76< W<14.85	2	7	1.100	0.178
14.85< W<30.000	3	8	1.100	0.178

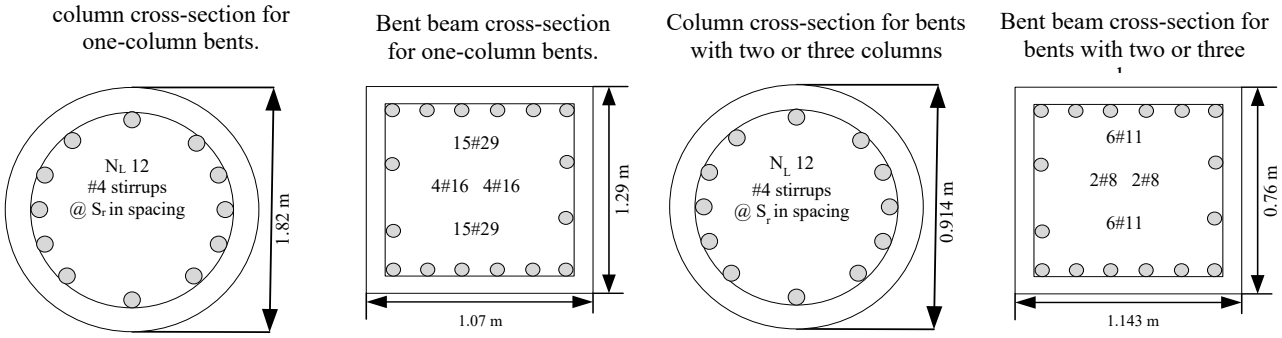

Fig. 2: configurations of columns and bent beams vary depending on the number of columns per bent.

The three-dimensional spine model of the bridges was created using the OpenSees simulation platform [26]. The interaction behavior between girders and the deck was modeled using the *ElasticBeamColumn* element available in the OpenSees simulation platform [26]. The column was evenly divided into 13 segments along its clear height. At the same time, the bent beam was divided into multiple components based on the number of girders, as shown in Table 1. Material uncertainties associated with the column and bent beam modeling were calculated as presented in Table 2. A *ZeroLength* element, combined with elastic material, was used to simulate the seismic behavior of the

foundation in both directions. To model the interaction between flexural and axial loads in columns and bent beams, distributed-plasticity fiber sections were assigned to the *dispBeamColumn* elements. Figure 3a illustrates the component's configuration in the abutment.

The consecutive behavior of reinforced bars was mimicked using *ReinforcingSteel* as presented in Figure 3b [27]. Based on the parametric variation outlined in Table 2**,** different parameters of ReinforcingSteel were determined. A value of 200 GPa was considered for the steel modulus of elasticity, while the ultimate strain ratio was assumed to be 0.12. The strain hardening ratio was assumed to be 2.0% of the steel's modulus of elasticity [28]. *Concrete07* was used to simulate both confined and unconfined concrete seismic behavior. More details about the consecutive behavior of *concrete07* are presented in Figure 3c [29]. Additionally, various uncertainty parameters of *concrete07* are presented in Table 2. Figure 3d shows the seismic behavior of the bearing pads mimicked by the *Steel01*. The initial stiffness of the bearing pads was computed using Eq. (1), and the yield strength characteristics were determined using Eq. (2). In these equations, A is the cross-sectional area of the base isolation, h is its thickness, N is the normal force applied to the bearing, G is the shear modulus of the bearing pad and μ is the coefficient of friction obtained using Eq. (3) [25]**.**

$$Kpad = \frac{GA}{h} \tag{1}$$

$$Fy = \mu N \tag{2}$$

$$\mu = 0.05 + \frac{0.4}{\sigma_n} \tag{3}$$

Shear keys were employed as sacrificed components to limit the transverse movement and protect components, as shown in Figure 3e [30]. *ElasticPPGap* and *MinMax* materials were used to capture the nonlinear behavior of the shear key. Whenever the *ElasticPPGap* material exceeded the specified capacity threshold, the *MinMax* material was used to restrict it. The shear key was designed to allow a maximum deformation of approximately 9 cm [30].

Table 2: Random variables and distributions incorporated in the bridge modeling.

Uncertainty parameter	Distribution	Mean	Dispersion	Min	Max
Middle span length [m]	Uniform	-	-	7.5	32.10
Column height [m]	Uniform	-	-	4.2	9.0
Deck width [m]	Uniform	-	-	10.0	30.0
Concrete unconfined strength [MPa]	Normal	33.8	4.3	-	-
Steel yield strength [MPa]	Lognormal	6.13	0.08	-	-
Longitudinal reinforcement ratio	Uniform	-	-	1.49	5.35
Transverse reinforcement ratio	Uniform	-	-	0.31	1.61
Bearing shear modulus [MPa]	Uniform	-	-	0.66	2.07
Friction multiplication factor	Lognormal	0.0	0.10		
Gap between deck and abutment [m]	Uniform	-	-	0.0	0.038
Gap between the deck and shear key [m]	Uniform	-	-	0.0	0.038
Height of the back wall [m]	Uniform	-	-	1.604	2.584
Gap between the adjacent deck[m]	Uniform	-	-	0.018	0.033
Cable yield strength [MPa]	Lognormal	7.1	0.30	-	-
Cable slack [m]	Uniform	-	-	0.006	0.0254
Cable length [m]	Uniform	-	-	2.40	6.10
Passive abutment stiffness [K.N./mm/m]	Uniform	-	-	11.5	28.8
Translational foundation stiffness [K.N. / mm]	Uniform	-	-	28.0	84.0
Rotational foundation stiffness [N-m/rad]	Uniform	-	-	$87.5e^6$	$262.5e^6$
Stiffness of the pile [K.N./mm]	Lognormal	2.63	0.30	-	-
Deck mass ratio	Uniform	-	-	1.10	1.40
Damping ratio	Normal	0.045	0.0125	-	-

To simulate the nonlinear behavior of the piles in both directions, hysteretic material was employed and assigned to ZeroLength (Figure 4a). Its ultimate deformation is assumed to be 2.54 cm, while the yielding deformation is 30% of the ultimate deformation. ZeroLength element along with ElasticPPGap was used to model restrainer cables in the OpenSees tool as presented in Figure 4b. Table 2 represents the parametric variations considered for modeling the restrainer cable. The seat-type abutment with passive and active resistance was employed, which could take into

consideration abutment walls to compress and move away from the backfill, respectively. Figure 4c depicts the hysteretic behavior of backfill soil modeled with *HyperbolicGap* material. More details about backfill modeling can be found in [1], [23], [31], [32]. Figure 4d shows the bilinear behavior of pounding mimicked via the two parallel *ElasticPPGap* materials. According to Nielsen's recommendations, the default parameter for the contact model was calculated.

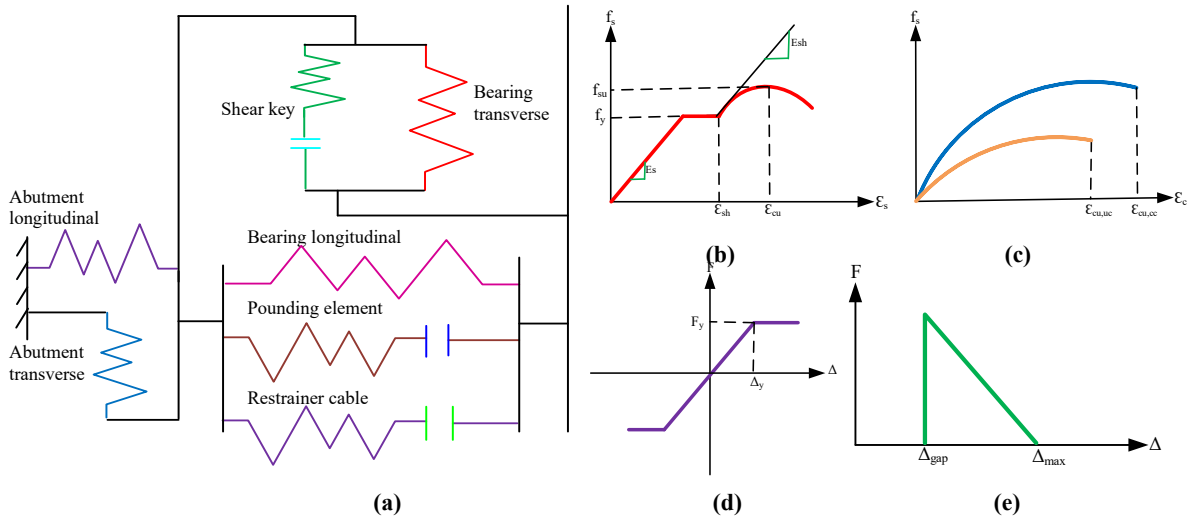

Fig. 3: (a) Abutment configurations, (b) reinforcement steel arrangement, (c) concrete specifications, (d) bearing pad components, and (e) shear key.

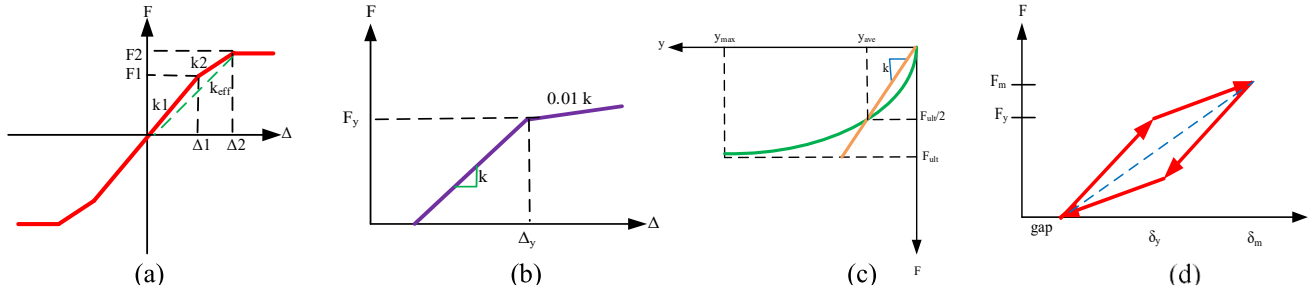

Fig. 4: Analytical representations developed for (a) piles, (b) restrainer cables, (c) soil behavior, and (d) pounding mechanisms within bridge structures.

3. Ground motion selection

In this study, to investigate the influence of local fire on the seismic behavior of MSSSS-IG bridges, NRHAs were implemented. As part of the ongoing research project, this ground motion dataset was used to develop a framework based on an ANN model to predict the response of bridge components subjected to earthquake and post-fire earthquake scenarios. For this reason, 160 input motion records were considered. These records were selected based on the recommendation of Baker et al. [33]. The datasets consist of a diverse range of input motions that have different characteristics of ground motions, including near-fault, far-field, long duration, short duration, and pulse-like. Figure 5 illustrates the response spectrum for all 160 records in both orthogonal directions and their statistics.

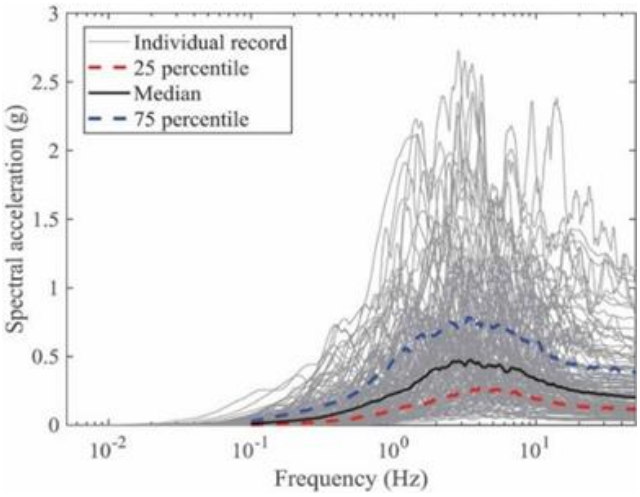

Fig. 5: Acceleration response for selected ground motion.

4. Simulation of fire

The primary objective of this study is to develop a demand model and generate fragility curves using the ANN algorithm for MSSSS-IG bridges subjected to localized fire exposure in columns. To achieve this, several steps are undertaken: conducting heat transfer analysis using the OpenSees Fire [34], determining the maximum temperature in the columns, applying stiffness and strength reduction factors to the fire-affected columns, and performing static analysis in OpenSees [26] to capture residual drifts and forces resulting from fire damage. Subsequently, NRHAs were conducted to generate a valuable dataset for training the ANN model to estimate the demand for components under the influence of localized fire in columns.

A two-step procedure was used to simulate fire exposure. This approach was developed based on the concept of stiffness and strength degradation [35-37]. Heat transfer analysis was conducted in the first phase, while degradation factors following Eurocode 2 [38] were derived and applied in the second step. In this study, a single column per bridge was considered exposed when the column was more than one the edge column was selected. The column experienced uniform heating along its entire length and through the full depth of its section. The fire influence on the bent beam was not considered since the significant capacity of the deck, girders, and the unaffected part of the bent beam.

A three-dimensional thermal analysis was conducted using the OpenSees Fire module [34]. A total of 1,600 ISO 834 fire curves were created, with peak temperatures uniformly distributed between 200 °C and 1,000 °C. Variations in column geometry and material properties were defined using the parameters described earlier. Table 3 presents the statistical distributions and ranges for specific heat and thermal conductivity. The *ConcreteEC2* model, developed based on Eurocode 2 [38], was used to model the thermal behavior of concrete. The concrete density was assumed to be 2,400 kg/m³, and the thermal properties were assigned based on the data from Kodur et al. [39], as listed in Table 3. The heat transfer model employed the *HTEntityBrick* element available in the OpenSees Fire module [34]. While temperature data were collected at multiple points along the column during the simulation, only the peak temperatures were used in subsequent analyses for simplification. These maximum temperatures are presented in Figure 6. Based on these peak values, degradation factors for concrete and steel materials were calculated in the second phase according to Eurocode 2 [38].

5. Machine learning generation

5.1 Linear regression algorithm

Multi-parameter LR is a popular regression technique that was utilized based on simplicity to achieve the best-fitting line through a data set [40]. A linear relationship was assumed between the dependent and independent features, which was applied to continuous-valued data. The line was fitted by minimizing the sum of the squared distances between the data points and the regression line. The estimation method of this model is by adding bias as a constant term to the weighted sum of the input features, as described by Eq. (4):

$$\hat{y} = \theta_0 + \theta_1 x_{1+} \theta_2 x_{2+},,, + \theta_n x_n \quad (4)$$

where $\hat{y}$ is the estimated value, n is the number of features, x_i is i^{th} feature value, and θ_j is j^{th} model parameter includes the bias term and the feature weights.

5.2 Artificial neural networks

ANNs are a rigorous ML model, which was developed based on inspiration from biological neuron systems. The architecture of ANNs includes four parts: layers, training algorithm, activation function, and neurons. Figure 6 depicts ANNs with four hidden layers and various neurons in each layer. A neural network requires at least an input layer, a hidden layer, and an output layer to be established. Depending on the purpose of the ANN model, the output layer may contain a single feature, multiple features for regression, or be structured for the classification task.

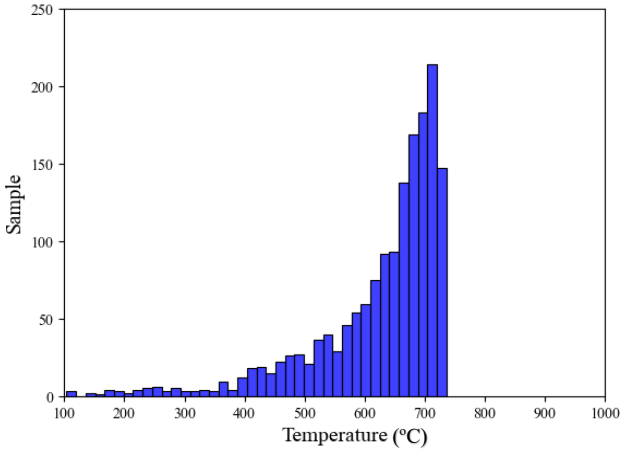

Fig. 6: Recorded peak temperature outcomes from the heat transfer analysis

Table 3: Stochastic variables and their associated probability distributions applied in the heat transfer analysis.

Uncertainty parameter	Unit	Distribution	Mean	Dispersion	References
Thermal conductivity	W/mk	Normal	1.33	0.37	[39]
Specific heat	W/mk	Normal	900	243	[39]

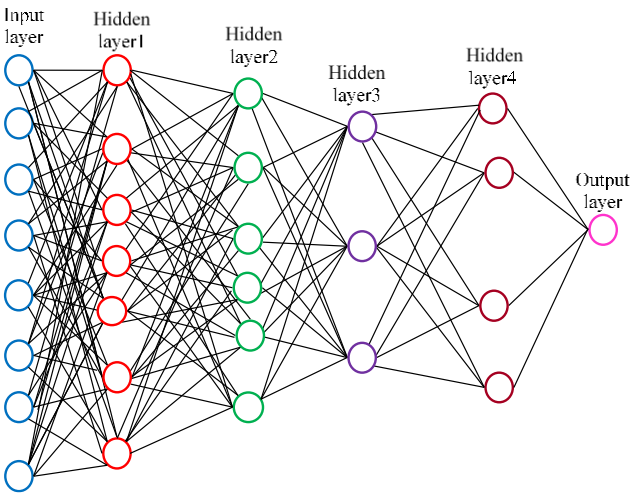

Fig. 7: The architecture of the artificial neural networks algorithm

The gradient descent, which is used for the first-order method or the second-order method, is widely used to train the ANN model. The first-order method was derived based on the first derivatives of the function to minimize, whereas the use of the Hessian matrix causes the generation of the second-order method. This study uses the first-order method to establish the ANN model, which could estimate the post-fire response of components. The decision of whether or not to activate a neuron is made by the activation function, which can be linear or nonlinear. Neurons processed the input variables by multiplying them with weights and adding a bias term as they passed from the input layer to the output layer.

Each neuron uses the following equation to determine activation ai and output values x_j:

$$xi = f(a_i) = f(\sum_j w_{ij} x_i - b) \quad (5)$$

In neural networks, the letter i stands for a neuron's layer that is now active, and the character j stands for the layer that is linked to the i_{th} neuron after it. The factors that affect how the neurons behave are x_i, f, $w_{ij,}$ and b, which stand for the input value, activation function, weight coefficient that determines the importance of the connection between the i_{th} and j_{th} neurons, and bias value, respectively. Together, these parameters create the complex relationships and calculations that neural networks do, which in turn shape the network's capacity for learning and prediction. Throughout the neural network's training, the values of w_{ij} and b may be modified iteratively.

For every neuron, the activation value ai is processed by the activation function f to provide the output value x_j. In the current study, the grid search was utilized to optimize the number of hidden layers, number of neurons, epoch, activation function, and the first-order training algorithm. The number of hidden layers was optimized between one and four, while the number of neurons in each hidden layer was set between 20 and 100. Moreover, the number of epochs ranged from 50 to 300. An epoch refers to a full cycle during which the entire training dataset is processed in one iteration. Table 4 lists the space of the activation function and first-order training algorithm, which is used as the space of optimization to train the ANNs. Note that to prevent overfitting, 5-fold cross-validation and dropout were applied.

5.3. Feature selection

Extreme gradient boosting (XGBoost) is an ensemble learning algorithm constructed from a series of decision trees (DTs) [41]. Each DT concentrates on fixing the errors in the prior tree so that the model may get more accurate over time by learning from its mistakes. Finding a feature's significance coefficient, which provides a weight depending on the model's sensitivity to the item feature, is another application of XGBoost [42-43]. This study employs the XGBoost model to assess feature importance. In this approach, each feature is treated as a decision node, and its significance during training is evaluated using the Gini impurity index.

Table 4: Space of activation function and optimizer.

Active function	Sigmoid, Softmax, Softplus, Softsign, Tanh, Expontional
	Exponential linear unit (Elu), Rectified linear unit (Relu)
Optimizer	Stochastic gradient descent (SGD)
	Root mean squared propagation (RMSprop)
	Adaptive Gradient Algorithm (AdaGrad)
	Adaptive moment estimation (Adam)
	Adaptive moment estimation with Weight Decay (AdamW)
	Adaptive learning rate method (Adadelta)
	Adaptive moment estimation maximum norm (Adamax)
	Nesterov accelerated gradient adaptive moment estimation (Nadam)

5.4. Assessment metrics

In the present investigation, three metrics were used to evaluate the effectiveness of the ANNs model: coefficient of determination (R^2), mean absolute error (MAE), and mean square error (MSE). The R^2 metric assessed how well the ANNs model fits the training data, MAE calculated the difference between anticipated and actual values, and MSE calculated the average of the squares of errors from predicted values. The following Equations represent the formulation of these criteria:

$$R^2 = \frac{\sum_{i=1}^{n}(\hat{y}_i - \bar{y}_i)^2}{\sum_{i=1}^{n}(y_i - \bar{y}_i)^2} \quad (6)$$

$$MAE = \frac{1}{n}\sum_{i=1}^{n}|y_i - \hat{y}_i| \quad (7)$$

$$MSE = \frac{1}{n}\sum_{i=1}^{n}(y_i - \hat{y}_i)^2 \quad (8)$$

Where y is the output of ML models, $\hat{y}$ is the actual label, $\overline{y}$ is the mean of the actual label, and n is the length.

6. Preprocessing

6.1. Generate data set

The current study aims to develop the fragility curves and predict the response of bridge components under an earthquake following fire using the ANNs algorithm. For this reason, 1600 MSSS-IG bridges were modeled using the OpenSees tool. The bridge samples were randomly paired with 160 ground motions scaled from 0.10g to 2.0g, and 62000 NRHAs were implemented for the pre-fire and earthquake following the fire to assess the remaining seismic capacity of the bridge subjected to fire.

6.2. Input variables

To develop an efficient ANN model, the input features must be comprehensive, incorporating uncertainties related to both bridges and input ground motions. The current study considers 42 input variables, including bridge types, ground motion intensity, and categorical features. Categorical features refer to characteristics that can be stored and identified based on qualitative data [40]. The categorical feature scenario type was utilized to take into account the effects of the two scenarios. 22 features of bridges based on parameter variations and 19 features corresponding to the intensity measures of earthquakes were considered. Table 5 lists the 42 input features used to develop the ANNs framework to predict the response of components and develop fragility curves under the impacts of earthquakes following a fire.

Table 5: List of input variables for the ANN model.

Variables	Definition	Variables	Definition
X_1	Scenario type	X_{22}	Bridge width
X_2	Peak ground acceleration	X_{23}	Column height
X_3	Peak ground velocity	X_{24}	Concrete unconfined strength
X_4	Peak ground displacement	X_{25}	Deck mass ratio
X_5	Root mean square acceleration	X_{26}	Steel yield strength
X_6	Root mean square velocity	X_{27}	Longitudinal reinforcement ratio
X_7	Root mean square displacement	X_{28}	Transverse reinforcement ratio
X_8	Arias Intensity	X_{29}	Friction multiplication factor
X_9	Characteristic Intensity	X_{30}	Rotational spring stiffnesses of the foundations
X_{10}	Cumulative absolute velocity	X_{31}	Translation spring stiffnesses of the foundations
X_{11}	Acceleration spectrum intensity	X_{32}	Bearing shear modulus
X_{12}	Velocity spectrum intensity	X_{33}	Gap between the deck and the shear key
X_{13}	Housner Intensity	X_{34}	Gap between the adjacent deck
X_{14}	Sustained maximum acceleration	X_{35}	Gap between the deck and the abutment
X_{15}	Sustained maximum velocity	X_{36}	Height of the back wall
X_{16}	Max incremental velocity	X_{37}	Passive soil resistance.
X_{17}	Standardized cumulative absolute velocity	X_{38}	Stiffness of the pile
X_{18}	Spectral acceleration at 0.2 sec.	X_{39}	Slack
X_{19}	Spectral acceleration at 1.0 sec.	X_{40}	Cable length
X_{20}	Spectral acceleration at the fundamental period	X_{41}	Cable yield strength
X_{21}	Bridge length	X_{42}	Damping ratio

6.3 Output Variables

Twelve components comprising the column, unseating, and many others are considered to develop fragility curves, as summarized in Table 6. The curvature ductility was considered to define the EDP in the column presented in Eq. (9):

$$\mu_\phi = \frac{\phi_u}{\phi_y} \quad (9)$$

where the ϕ_u and ϕ_y is yield curvature and ultimate curvature, respectively. The displacement in the longitudinal and transverse direction was regarded as the EDP for unseating and deck transverse movement, respectively. For abutments in the active, transverse, and passive directions, the corresponding displacement was used as an EDP, and the displacement in the translation direction and rotational direction were utilized as EDPs in the foundation, respectively. To the bearing pad in the longitudinal and transverse direction, the corresponding displacements are employed as EDPs. Table 6 lists the EDPs for different components used to create the PSDM.

Primary structural elements play a major role in the bridge's vertical stability and load-bearing capacity, while secondary components have a comparatively lesser influence. Columns and deck seating at the abutments are classified as primary components, whereas the remaining elements are considered secondary. The correlation between component demands is assessed for each bridge type in all scenarios to develop a joint probabilistic seismic demand model (JPSDM) for generating the system fragility curves. As suggested by HAZUS [44], several damage states are employed in this study to categorize the members' capabilities. The damage states consist of light, moderate, extensive, and complete levels, corresponding to DS1, DS2, DS3, and DS4, respectively. The capacity of components in different damage states is outlined in Table 8.

Table 6: List of output variables for the machine-learning model.

ID	Components	EDP	Variables	ID	Components	EDP	Variables
1	Column	Curvature	log(μ)	7	Deck.tran	Displacement	log(δ)
2	Abt.seat	Displacement	log(δ)	8	Fnd.tran	Displacement	log(δ)
3	Brg.long	Displacement	log(δ)	9	Fnd.rot	Rotation	log(θ)
4	Brg.tran	Displacement	log(δ)	10	Abt.pass	Displacement	log(δ)
5	Cable	Displacement	log(δ)	11	Abt.act	Displacement	log(δ)
6	Shear key	Displacement	log(δ)	12	Abt.tran	Displacement	log(δ)

Table 7: Damage states adopted for various components in this study.

Component	Units	DS1	β_c	DS2	β_c	DS3	β_c	DS4	β_c
Columns		1	0.35	4	0.35	8	0.35	12	0.35
Abt.seat	mm	25.4	0.35	76.2	0.35	152.4	0.35	228.6	0.35
Brg.long	mm	25.4	0.35	101.6	--	--	--	--	--
Brg.tran	mm	25.4	0.35	101.6	--	--	--	--	--
Restrainer cables	mm	38.1	0.35	101.6	--	--	--	--	--
Shear key	mm	38.1	0.35	127	--	--	--	--	--
Deck.tran	mm	101.6	0.35	304.8	--	--	--	--	--
Fnd.tran	mm	25. 4	0.35	101.6	--	--	--	--	--
Fnd.rot	radian	1.5	0.35	6	--	--	--	--	--
Abt.pass	mm	76.2	0.35	254	--	--	--	--	--
Abt.act	mm	38.1	0.35	101.6	--	--	--	--	--
Abt.tran	mm	25.4	0.35	101.6	--	--	--	--	--

Table 8: Results of grid research to develop the architecture of ANN.

Components	Active function	Optimizer	Number of input and hidden layers	Number of neurons in each hidden layer	Epoch
Column	Relu	Adam	2	70	300
Abt.seat	Relu	RMSprop	4	100	100
Brg.long	Softsign	Nadam	2	100	300
Brg.tran	Relu	Adam	2	100	200
Cable	Tanh	Adam	4	50	150
Deck	Relu	Adamax	2	70	250
Shear	Relu	Adam	3	100	200
Fnd.rot	Relu	Nadam	3	70	250
Fnd.tran	Relu	Adam	3	100	300
Abt.pass	Relu	Nadam	4	70	100
Abt.act	Relu	Adam	3	100	100
Abt.tran	Relu	Adam	2	100	200

7. Results and discussion

Table 9 illustrates the outcome of the grid search to determine the hyperparameters of the bridge component. As shown, in all elements except the bearing in the longitudinal direction and the restrainer cable, the rectified linear unit (Relu) is an ideal activation function, which reveals the efficiency of Relu for developing the ANN model. In the bearing in the longitudinal direction, the Softsign function is more reliable, while in the cable, the Tanh is more suitable. In all components except the longitudinal movement of the deck (unseating), the Adam optimizer or optimizer is developed based on the Adam, including Adamax exhibits better performance, and becomes the optimal optimizer in the ANNs algorithm. The grid search finding indicates that any of the elements cannot reach a suitable prediction performance with one hidden layer. Furthermore, the grid search outcomes in selecting the number of hidden layers have been confirmed by the results of the number of neurons in each hidden layer and epoch, which reveal that increasing the complexity of ANNs causes results to be more effective. The results of components subjected to the effect of pre- and post-fire using the ANNs model in terms of R^2, MSE, and MAE are illustrated in Table 9. In all members except active soil in the test set, the R^2 is more than 90%, which shows the power of the ANN model to estimate the outcome of elements. The results of MAE and MSE also confirm the finding of R^2 in the various conditions, which demonstrates the efficiency of all assessment metrics in developing a framework to predict the response of components under pre- and post-fire scenarios in the MSSSS-IG bridge.

Moreover, the difference between test and train set data is less than or equal to 3%, revealing that overfitting did not occur. The ANN model has better prediction performance in the primary components for the column, while it has promising performance for the foundation in the rotational direction in the secondary components. The comparison between the former and the latter highlights that in terms of R^2, the result is equal, whereas in terms of MAE and MSE, the ANNs have better performance in the latter, as shown in Table 9. The outcome bearing indicates that the ANN model has suitable performance in the longitudinal direction, with higher R^2 and lower MSE and MAE compared to the transverse direction. The ANNs have a better estimation of the response of passive movement of the abutment compared to transverse and active movement.

Table 9: Results of ANNs for full features.

Components	R^2(%)		MAE (10^{-2})		MSE (10^{-3})	
	Train	Test	Train	Test	Train	Test
Column	99.6	99.0	4.17	4.51	4.51	5.18
Unseating	98.0	96.0	4.15	4.71	6.74	11.9
Brg.long	97.4	96.0	5.97	6.87	14.9	22.2
Brg.tran	95.3	94.5	7.72	8.63	15.2	19.5
Cable	96.0	96.0	6.31	6.69	11.7	12.2
Deck.tran	98.4	98.0	4.75	5.09	6.95	7.06
Fnd.rot	99.0	99.0	3.13	3.34	2.32	2.74
Fnd.tran	97.3	94.5	3.29	3.81	5.38	9.72
Abt.pass	96.5	95.2	9.04	9.89	22.4	26.8
Abt.act	91.0	88.8	9.48	10.8	24.9	33.5
Abt.tran	95.2	93.6	9.36	10.3	20.5	25.4

Table 10 displays the top 15 features of various components, obtained based on an approach of feature significance via the XGBoost technique. As shown in all components, the scenario type is an essential feature. As mentioned earlier, the scenario type is a categorical feature that is used to take into consideration the post- and pre-fire scenarios. These findings highlight the importance of fire in the seismic performance of bridges. The feature selection shows that the

arias intensity (AI), characteristic intensity (CI), and cumulative absolute velocity (CAV) for most of the components are important intensity measures. Additionally, in all elements, velocity spectrum intensity (VSI), Housner intensity (HI), spectral acceleration at 1.0 sec (Sa(1.00)), and spectral acceleration at the fundamental period of bridges ($Sa(T_1)$) are significant features.

In addition, it can be found that displacement-related intensities like peak ground displacement and root mean square displacement have little effect, as outlined in Table 10. This outcome shows the lousy performance of displacement-related intensity to predict the response of components under an earthquake following a fire. The bridge width and bridge length in all members except the column are ideal features based on the result of the XGBoost model, as well as the column height in all components except the foundation in the rotational direction is a vital feature. These findings reveal the importance of bridge geometry in the seismic performance of bridges.

Table 10: Top 15 features based on the random shuffling approach.

Components	Top 15 features
Column	X_1, X_8, X_{10}, X_{12}, X_{13}, X_{17}, X_{19}, X_{20}, X_{23}, X_{26}, X_{27}, X_{32}, X_{33}, X_{34}, X_{42}.
Abt.seat	X_1, X_8, X_9, X_{11}, X_{12}, X_{13}, X_{19}, X_{20}, X_{21}, X_{22}, X_{23}, X_{27}, X_{28}, X_{32}, X_{42}.
Brg.long	X_1, X_9, X_{11}, X_{12}, X_{13}, X_{19}, X_{20}, X_{21}, X_{22}, X_{23}, X_{27}, X_{32}, X_{34}, X_{38} X_{42}.
Brg.tran	X_9, X_{11}, X_{12}, X_{13}, X_{19}, X_{20}, X_{21}, X_{22}, X_{23}, X_{30}, X_{32}, X_{33}, X_{38}, X_{40}, X_{42}.
Cable	X_1, X_{10}, X_{11}, X_{12}, X_{13}, X_{19}, X_{20}, X_{21}, X_{22}, X_{23}, X_{32}, X_{33}, X_{38}, X_{39}, X_{42}.
Shear key	X_1, X_9, X_{10}, X_{11}, X_{12}, X_{13}, X_{19}, X_{20}, X_{21}, X_{22}, X_{23}, X_{30}, X_{32}, X_{33}, X_{42}.
Deck.tran	X_1, X_{10}, X_{11}, X_{12}, X_{13}, X_{19}, X_{20}, X_{21}, X_{22}, X_{23}, X_{30}, X_{32}, X_{33}, X_{38}, X_{42}.
Fnd-tran	X_1, X_{10}, X_{11}, X_{12}, X_{13}, X_{19}, X_{20}, X_{21}, X_{22}, X_{23}, X_{26}, X_{27}, X_{30}, X_{31}, X_{32}.
Fnd.rot	X_1, X_{11}, X_{12}, X_{13}, X_{19}, X_{20}, X_{21}, X_{22}, X_{27}, X_{30}, X_{32}, X_{34}, X_{36}, X_{40}, X_{42}.
Abt.pas	X_1, X_{12}, X_{13}, X_{19}, X_{20}, X_{21}, X_{22}, X_{23}, X_{32}, X_{33}, X_{36}, X_{37}, X_{38}, X_{39}, X_{42}.
Abt.act	X_1, X_{10}, X_{12}, X_{13}, X_{14}, X_{15}, X_{17}, X_{19}, X_{20}, X_{21}, X_{22}, X_{23}, X_{32}, X_{38}, X_{39}.
Abt.tran	X_1, X_{12}, X_{13}, X_{19}, X_{20}, X_{21}, X_{22}, X_{23}, X_{28}, X_{32}, X_{33}, X_{35}, X_{38}, X_{39}, X_{42}.

The result of the ANNs model using the top 15 features to predict the response of the primary component is illustrated in Figure 8. As shown, when the results are compared to Table 9, it can be observed that the decreases of input feature have insignificant effects in terms of R^2 in the column for both the train and test set. At the same time, the train and test sets of unseating 1% declined due to eliminating the redundant features. However, the error in terms of MSE and MAE increases in the column and unseating. Moreover, the outcomes show that proposed ANNs with the highest accuracy and the lowest error reduce the computational cost estimate of the demand for columns and unseating. As can be seen, the proposed approach estimates the demand of columns with R^2 values of 99.6% and 99.0% for the train and test set data, respectively. These values of R^2, reducing between 2% and 3%, are recorded for unseating.

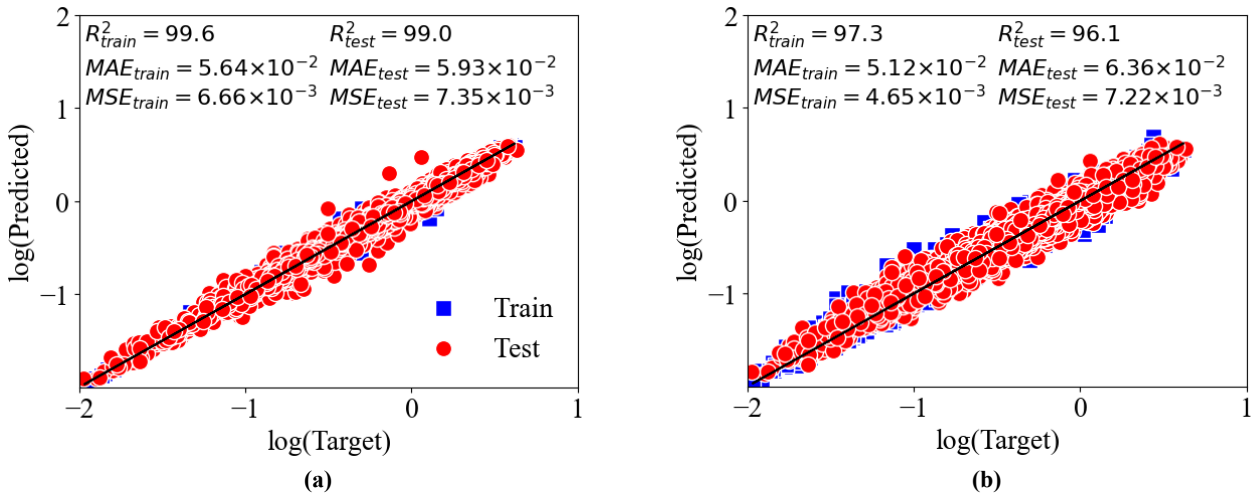

Fig. 8: Results of developing demand models for primary components. (a) Columns, (b) Unseating

Figure 9 illustrates the outcomes of the developed demand model based on significant features in the secondary components. The findings highlight that 1% of R^2 declines in both directions in the train and test sets. In the restrainer cable, the performance due to the elimination of the redundant feature is reduced by 1% and 2% for the train and test sets, respectively. The outcomes of developed ANNs based on top features demonstrate that the shear key is sensitive to the reduction of characteristics. In the shear key, the R^2 decreases around 6% and 4% for the train set and test set, respectively. The decreases in the R^2 did not occur in the foundation in the rotational direction, highlighting that the foundation is rigorous to feature elimination as illustrated in Figure 9. In conclusion, the results demonstrate that the removal of the 27 input features has an insignificant impact on the performance of the ANN model.

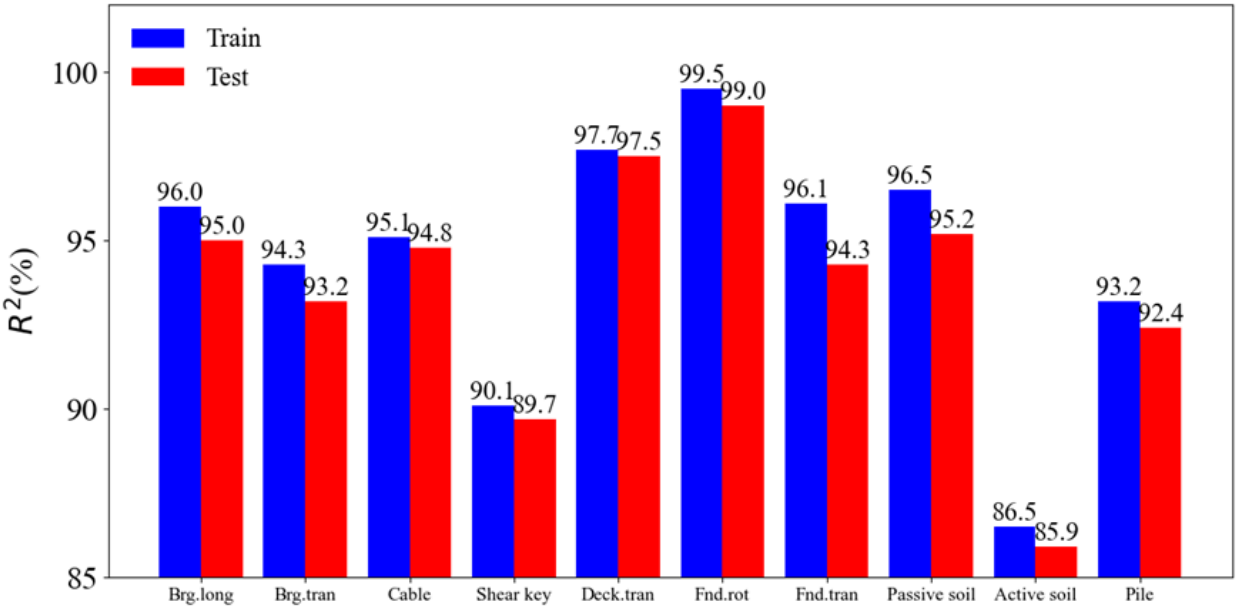

Fig. 9: Results of developing demand models for secondary components.

The primary reason for developing the ANN model is to increase the prediction performance, while using ANNs increases the complexity of the model for the estimation of component responses. Employing the feature selection eliminates the redundant characterization of the complexity of model decline. However, sometimes, the decrease in complexity may cause the ANN model to become inefficient. The multi-parameter LR algorithm typically has the lowest computational cost and complexity, and periodically estimates the model's response well, so there is no need to develop complex models. However, the outcome of the ANN model to assess the efficiency and better performance against the multi-parameter LR method is compared. Figure 10 compares the ANN model against multi-parameter LR in terms of R^2, MAE, and MSE for all components. As shown, ANNs achieved better prediction performance on average of more than 30% compared to multi-parameter LR based on the R^2 metric. This finding highlights the efficiency of ANNs compared to the LR algorithm, which is the traditional approach to developing the demand model.

The current research considers the vulnerability of multiple components, including columns, deck seating, bearings, shear key, restrainer cable, foundations, and abutments. The developed fragility curves for primary and secondary components-based ANN models using significant features for pre- and post-fire scenarios are presented in Figure 11 and Figure 12, respectively. Moreover, the median and dispersion of both scenarios outlined in Table 11. Note that, based on the results of a previous study, Sa(T1) is considered to develop the fragility curves. Overall, results demonstrate that while only one column is subjected to fire, fire has a detrimental impact on most of the components. This finding highlights the significance of fire in the seismic performance of bridge components.

Concerning Table 11, it can be found that the local fire reduces the capacity of the column between 11.0% and 12.0% across all damage states. In addition, it can be observed that the cable is sensitive to the local fire in the column. This is mainly due to the high correlation between the components of bridges. However, the results of developing the fragility curves in components of bridges for both scenarios show that the foundation and active soil are resistant to both fire and earthquakes in DS1. Meanwhile, it can be observed in DS2 that active soil, pile, passive soil, and foundation are not sensitive to either fire or earthquake. The result revealed that columns are the vulnerable components of bridges in all scenarios, and their stability plays the most significant role in bridge performance. In this scenario, one column is directly exposed to fire and loses its

stiffness and strength. Considering that the aim of this assessment is the seismic behavior of post-fire bridges and the volume of the fire in the bridge is limited, the results obtained for the fire at the location girder (scenario 2), in which the column is the most vulnerable member, are reasonable. In other words, it can be said that the failure mode of the bridges does not change because the fire's volume is limited; if the fire's volume increases, the obtained results may change.

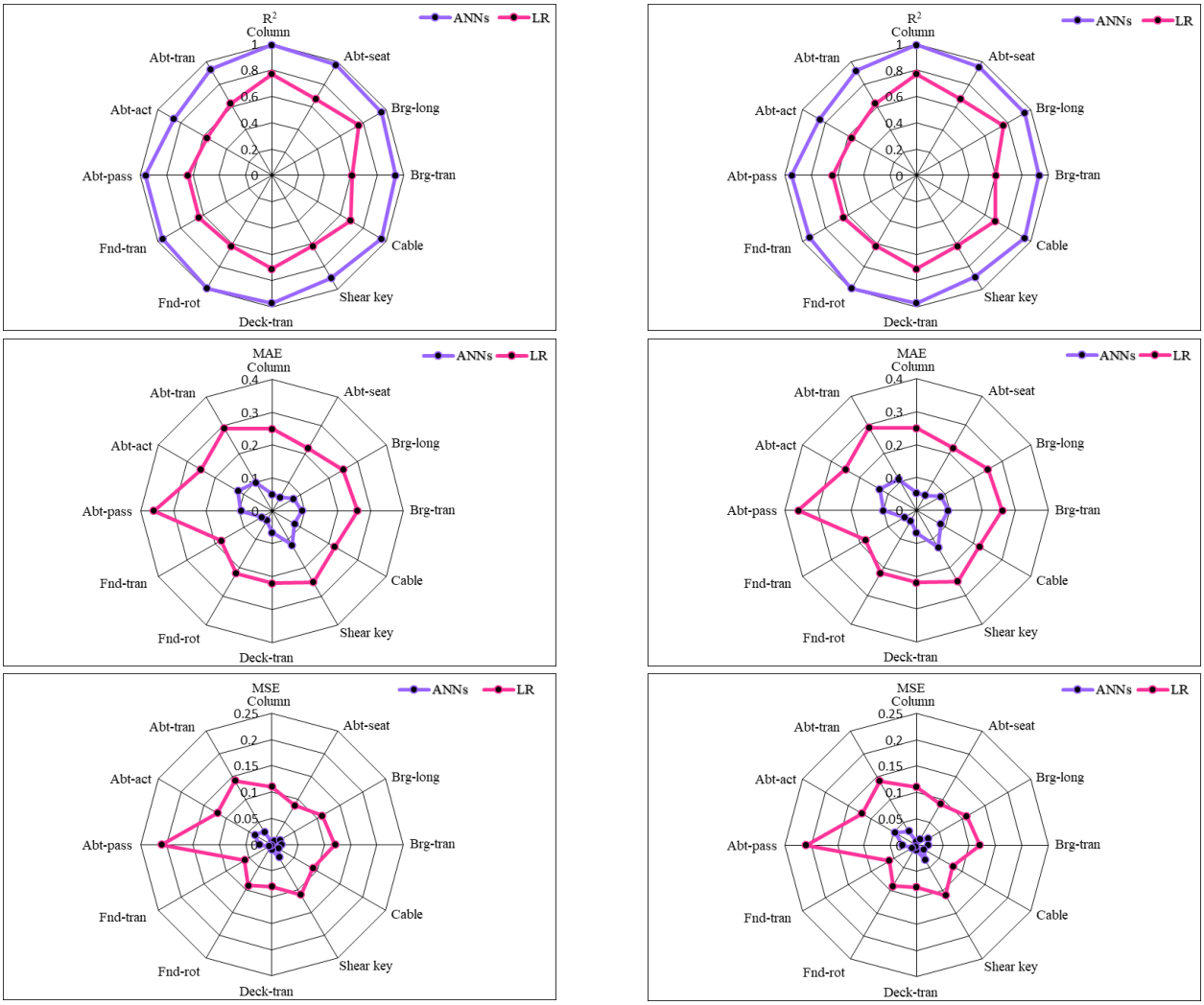

Fig. 10: Architecture of an artificial neural network algorithm.

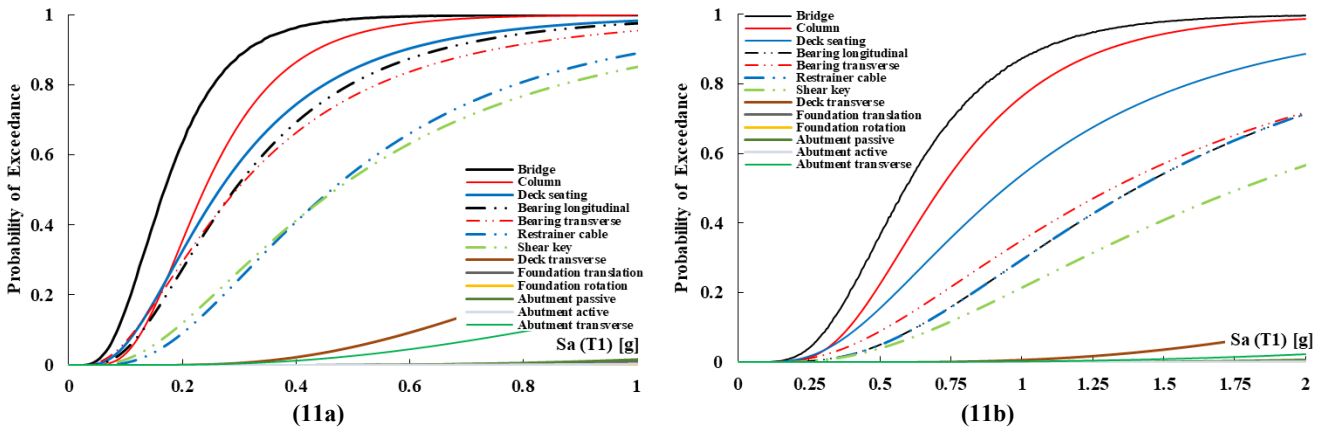

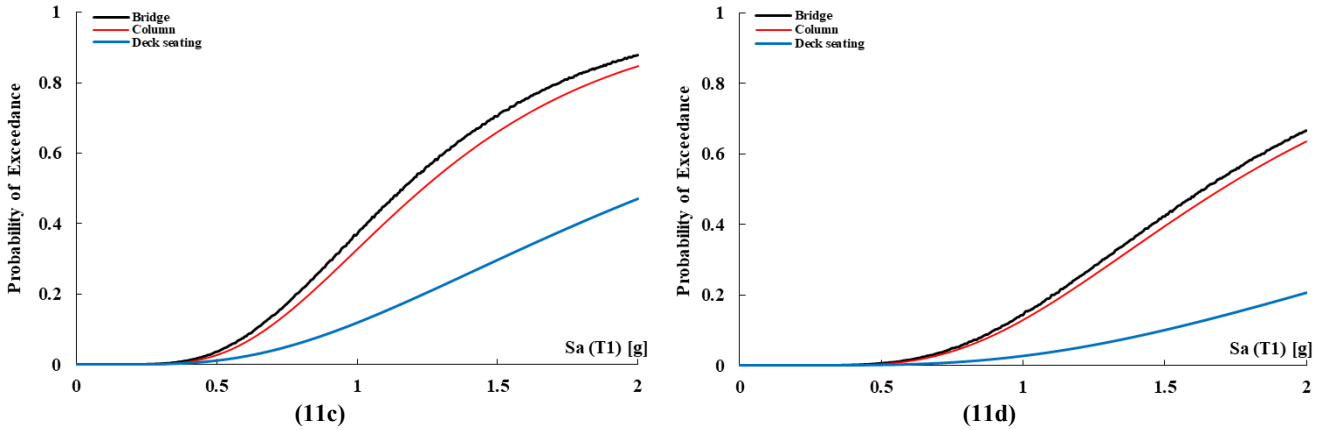

Fig. 11: Fragility curve for system and components of multi-span simply supported steel girder bridges in different damage states subjected to the earthquake. (a) Slight, (b) Moderate, (c) Extensive, (d) Complete

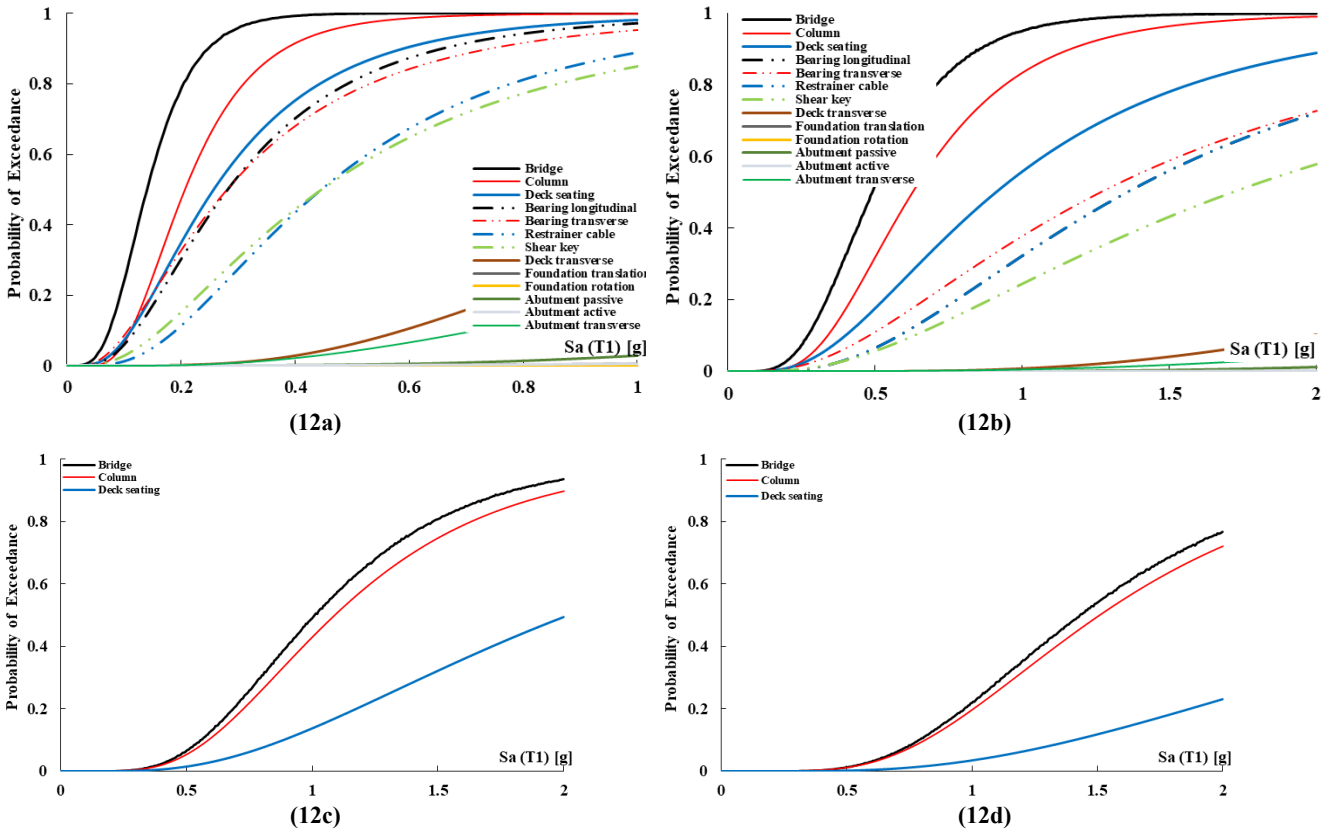

Fig. 12: Fragility curve for system and components of multi-span simply supported steel girder bridges in different damage states subjected to fire in the column following the earthquake. (a) Slight, (b) Moderate, (c) Extensive, (d) Complete

Fragility findings for the system level of bridges in all damage states are outlined in Table 12. Generally, outcomes show that the bridge system is sensitive to local fire in the column. This is mainly because the column is the critical component of the bridge, and changes in the capacity of the column significantly impact the system level of bridges. It can be found that the proposed ANN model develops the fragility curves for the system level of bridges with a median of failure 0.17 g, 0.59 g, 1.16 g, and 1.63 g when damage reaches DS1, DS2, DS3, and DS4, respectively. With reference to Table 12, it can be observed that these values of the median with 17.6%, 22.3%, 12.9%, and 12.3% reduction are reached at 0.14 g, 0.46 g, 1.01 g, and 1.43 g in those damaged states. This means that the bridge system level is more sensitive to local fires in columns compared to components. In conclusion, this finding reveals the significance of local fire in the seismic performance of the bridge, even if one column is subjected to fire.

Table 11: Component fragility curves in different scenarios.

Component	Scenario	Med (g)	Diff (%)	Disp (g)	Med (g)	Diff (%)	Disp (g)	Med (g)	Diff (%)	Disp (g)	Med (g)	Diff (%)	Disp (g)
Column	Pre-fire	0.24	0.00	0.27	0.71	0.00	0.27	1.23	0.00	0.27	1.70	0.00	0.32
	Post-fire	0.21	12.5	0.28	0.63	١١.0	0.28	1.09	١١٫۴	0.22	1.51	١١٫٢	0.31
Abt.seat	Pre-fire	0.27	0.00	0.32	0.94	0.00	0.32	2.09	0.00	0.28	3.33	0.00	0.25
	Post-fire	0.26	3.70	0.34	0.91	٣٫٢0	0. 34	2.02	٣٫۴0	0.25	3.22	٣٫٣0	0.25
Brg.long	Pre-fire	0.29	0.00	0.33	1.40	0.00	0. 33	--	--	--	--	--	--
	Post-fire	0.28	3.40	0.36	1.35	٣٫۶0	0. 36	--	--	--	--	--	--
Brg.tran	Pre-fire	0.30	0.00	0.32	1.32	0.00	0. 32	--	--	--	--	--	--
	Post-fire	0.28	6.67	0.36	1.27	٢٫٨0	0. 36	--	--	--	--	--	--
Cable	Pre-fire	0.46	0.00	0.33	1.40	0.00	0. 33	--	--	--	--	--	--
	Post-fire	0.45	2.10	0.36	1.35	٣٫۶0	0. 36	--	--	--	--	--	--
Shear key	Pre-fire	0.47	0.00	0.33	1.78	0.00	0. 33	--	--	--	--	--	--
	Post-fire	0.45	4.30	0.38	1.72	٣٫۴0	0. 38	--	--	--	--	--	--
Deck.tran	Pre-fire	1.34	0.00	0.31	4.45	0.00	0. 31	--	--	--	--	--	--
	Post-fire	1.30	٣.00	0.31	4.37	٢٫٩0	0. 31	--	--	--	--	--	--
Fnd.tran	Pre-fire	٩٩.0	0.00	0.00	٩٩.0	0.00	0.00	--	--	--	--	--	--
	Post-fire	٩٩.0	0.00	0.00	٩٩.0	0.00	0.00	--	--	--	--	--	--
Fnd.rot	Pre-fire	٩٩.0	0.00	0.00	٩٩.0	0.00	0.00	--	--	--	--	--	--
	Post-fire	٩٩.0	0.00	0.00	٩٩.0	0.00	0.00	--	--	--	--	--	--
Abt.pass	Pre-fire	4.25	0.00	0.38	٩٩.0	0.00	0.00	--	--	--	--	--	--
	Post-fire	3.90	٨٫٢0	0.32	٩٩.0	0.00	0.00	--	--	--	--	--	--
Abt.act	Pre-fire	٩٩.0	0.00	0.00	٩٩.0	0.00	0.00	--	--	--	--	--	--
	Post-fire	٩٩.0	0.00	0.00	٩٩.0	0.00	0.00	--	--	--	--	--	--
Abt.tran	Pre-fire	2.11	٠.00	0.34	٩٩.0	0.00	0.00	--	--	--	--	--	--
	Post-fire	1.99	٨٫۴0	0.40	٩٩.0	0.00	0.00						

Table 12: System fragility curves in different scenarios.

Scenarios	Med (g)	Diff (%)	Disp (g)	Med (g)	Diff (%)	Disp (g)	Med (g)	Diff (%)	Disp (g)	Med (g)	Diff (%)	Disp (g)
Pre-fire	0.17	٠.00	0.50	0.59	٠.00	0.49	1.16	٠.00	0.47	1.63	٠.00	0.47
Post-fire	0.14	17.6	0.46	0.46	22.3	0.45	1.01	12.9	0.46	1.43	12.3	0.47

8. Conclusion

This paper presented a framework for predicting the bridge component's responses and developing the fragility curves subjected to pre- and post-fire based on the ANN model. For this purpose, the LHS was employed, and MSSSS-IG bridges were created using the OpenSees simulation platform. Each of the 1600 bridges was randomly paired with uniformly distributed temperatures for component columns. A suite of 160 input motions scaled from 0.10g to 2.0g was considered. The 62,000 nonlinear response history analyses were performed for post- and pre-fire scenarios. Then, a grid search was used to optimize the hyperparameters of the ANNs' algorithms. The top 15 features were determined based on the XGBoost importance approach to reduce the complexity of the ANN model. The primary findings of this study are as follows:

- The outcome of the grid search highlights that the Relu and Adam optimizers are powerful activation functions and optimizers, respectively. Additionally, it increases the ANN complexity by employing the number of neurons and adding more hidden layers to improve the prediction performance of components.
- The ANN model developed utilizing full features appropriately estimates the response of components, and except for active soil in the test set, the R^2 is equal to or more than 90%.

- The result of feature selection based on the XGBoost importance approach reveals that in all components, the VSI, HI, Sa(1.00), and Sa(T_1) are significant features. Furthermore, in most of the components, the geometry of bridges has a substantial impact on the ANN model.
- Feature selection appropriately demonstrates the importance of fire in the seismic performance of the components exposed to fire.
- The effects of feature elimination in the prediction performance of the generated ANNs model using the top 15 features are negligible, and in the critical condition, only 6% of R^2 declined.
- The result shows that ANNs are more potent than multi-parameter linear regression in estimating the response of components.
- Fragility results at the component level reveal the significant impact of localized fire on the seismic performance of most bridge components, particularly columns and cables.
- Fragility outcomes at the system level indicate that localized fire in columns reduces the overall seismic performance of bridges by approximately 12% to 22%.

8.1 Use of Results in Practice

The results of this study show that even a localized fire in one column can significantly reduce the seismic performance of bridges. The proposed ANN-based framework can be used as a practical tool for predicting the post-fire behavior of bridge components and the entire system. These findings can help engineers to better evaluate fire-damaged bridges and make informed decisions about retrofitting and risk reduction, especially for critical elements like columns and cables.

8.2 Recommendations for future research

For future work, it is recommended to use more advanced machine learning methods such as deep learning or graph-based models to improve prediction accuracy. Also, considering non-uniform and spreading fire scenarios can make the analysis closer to real conditions. The same framework can also be tested on other bridge types or applied at the network scale. In addition, combining the model results with real post-fire inspection data can improve its practical value and reliability.

9. References

[1] N. Rabiee, S. Shiravand, and S. Soroushian, "Post-fire seismic capacity estimation using temperature-varying fragility curve in bridges," *Structures*, vol. 76, no. March, p. 108876, 2025, doi: 10.1016/j.istruc.2025.108876.

[2] W. Wright, B. Lattimer, M. Woodworth, M. Nahid, and E. Sotelino, "Highway Bridge Fire Hazard Assessment," no. 12, 2013.

[3] G. C. Lee, S. B. Mohan, C. Huang, and B. N. Fard, "A study of US bridge failures," 2013.

[4] J. Alos-Moya, I. Paya-Zaforteza, A. Hospitaler, and P. Rinaudo, "Valencia bridge fire tests: Experimental study of a composite bridge under fire," *J. Constr. Steel Res.*, vol. 138, pp. 538–554, 2017, doi: 10.1016/j.jcsr.2017.08.008.

[5] J. Hu, A. Usmani, A. Sanad, and R. Carvel, "Fire resistance of composite steel & concrete highway bridges," *J. Constr. Steel Res.*, vol. 148, pp. 707–719, 2018, doi: 10.1016/j.jcsr.2018.06.021.

[6] C. Cui, A. Chen, and R. Ma, "Stability assessment of a suspension bridge considering the tanker fire nearby steel-pylon," *J. Constr. Steel Res.*, vol. 172, p. 106186, 2020, doi: 10.1016/j.jcsr.2020.106186.

[7] M. Ok, K. Kim, J. Hyun, and M. Kyum, "Fire risk assessment of cable bridges for installation of firefighting facilities," vol. 115, 2020.

[8] R. Ma, C. Cui, M. Ma, and A. Chen, "Numerical simulation and simplified model of vehicle-induced bridge deck fire in the full-open environment considering wind effect," *Struct. Infrastruct. Eng.*, vol. 17, no. 12, pp. 1698–1709, 2021, doi: 10.1080/15732479.2020.1832535.

[9] G. Peris-Sayol, I. Paya-Zaforteza, J. Alos-Moya, and A. Hospitaler, "Analysis of the influence of geometric, modeling and environmental parameters on the fire response of steel bridges subjected to realistic fire scenarios," *Comput. Struct.*, vol. 158, pp. 333–345, 2015, doi: 10.1016/j.compstruc.2015.06.003.

[10] C. Song, G. Zhang, V. Kodur, Y. Zhang, and S. He, "Fire response of horizontally curved continuous composite bridge girders," *J. Constr. Steel Res.*, vol. 182, p. 106671, 2021, doi: 10.1016/j.jcsr.2021.106671.

[11] J. Hu, R. Carvel, and A. Usmani, "Bridge fires in the 21st century: A literature review," *Fire Saf. J.*, vol. 126, no. February, p. 103487, 2021, doi: 10.1016/j.firesaf.2021.103487.

[12] B. Behnam and H. Ronagh, "Performance of reinforced concrete structures subjected to Fire following earthquake," *Eur. J. Environ. Civ. Eng.*, vol. 17, no. 4, pp. 270–292, 2013, doi: 10.1080/19648189.2013.783882.

[13] M. Memari, H. Mahmoud, and B. Ellingwood, "Post-earthquake fire performance of moment resisting frames with reduced beam section connections," *J. Constr. Steel Res.*, vol. 103, pp. 215–229, 2014, doi: 10.1016/j.jcsr.2014.09.008.

[14] S. Ni and A. C. Birely, "A simplified model for the post-fire earthquake flexural response of reinforced concrete walls with boundary elements," *Eng. Struct.*, vol. 175, no. July, pp. 721–730, 2018, doi: 10.1016/j.engstruct.2018.08.044.

[15] Y. Deng, M. Zhang, D. M. Feng, and A. Q. Li, "Predicting fatigue damage of highway suspension bridge hangers using weigh-in-motion data and machine learning," *Struct. Infrastruct. Eng.*, vol. 17, no. 2, pp. 233–248, 2021, doi: 10.1080/15732479.2020.1734632.

[16] N. Hider, A. Marahlleh, H. Liu, A. M. Asce, O. Abudayyeh, and M. Asce, "Deterioration Prediction Models for the Condition Assessment of Concrete Bridge Decks Using Machine Learning Techniques," 2015.

[17] Y. Shi, L. Xiong, H. Qin, J. Han, and Z. Sun, "Seismic fragility analysis of LRB-isolated bridges considering the uncertainty of regional temperatures using BP neural networks," *Structures*, vol. 44, no. August, pp. 566–578, 2022, doi: 10.1016/j.istruc.2022.08.035.

[18] Z. Wang, W. Zhang, Y. Zhang, and Z. Liu, "Temperature Prediction of Flat Steel Box Girders of Long-Span Bridges Utilizing In Situ Environmental Parameters and Machine

Learning," *J. Bridg. Eng.*, vol. 27, no. 3, pp. 1–18, 2022, doi: 10.1061/(asce)be.1943-5592.0001840.

[19] F. Wedel and S. Marx, "Application of machine learning methods on real bridge monitoring data," *Eng. Struct.*, vol. 250, no. February 2021, p. 113365, 2022, doi: 10.1016/j.engstruct.2021.113365.

[20] V. K. Kodur and M. Z. Naser, "Classifying bridges for the risk of fire hazard via competitive machine learning," *Adv. Bridg. Eng.*, vol. 2, no. 1, 2021, doi: 10.1186/s43251-020-00027-2.

[21] J. Feng, K. Gao, W. Gao, Y. Liao, and G. Wu, "Machine learning-based bridge cable damage detection under stochastic effects of corrosion and fire," *Eng. Struct.*, vol. 264, no. January, p. 114421, 2022, doi: 10.1016/j.engstruct.2022.114421.

[22] E. Aziz and V. Kodur, "An approach for evaluating the residual strength of fire exposed bridge girders," *J. Constr. Steel Res.*, vol. 88, pp. 34–42, 2013, doi: 10.1016/j.jcsr.2013.04.007.

[23] S. Shiravand, N. Rabiee, and S. Soroushian, "Fuzzy analytical hierarchy process and component importance measures for selection optimal intensity measures and development fragility curves in bridges," *Soil Dyn. Earthq. Eng.*, vol. 194, no. February, p. 109352, 2025, doi: 10.1016/j.soildyn.2025.109352.

[24] K. Ramanathan, J. E. Padgett, and R. DesRoches, "Temporal evolution of seismic fragility curves for concrete box-girder bridges in California," *Eng. Struct.*, vol. 97, pp. 29–46, 2015, doi: 10.1016/j.engstruct.2015.03.069.

[25] K. N. Ramanathan, "Next generation seismic fragility curves for california bridges incorporating the evolution in seismic design philosophy," 2012.

[26] S. Mazzoni, F. Mckenna, M. Scott, and G. Fenves, "OpenSees Command Language Manual," *Pacific Earthq. Eng. Res. Cent.*, vol. 264, no. 1, pp. 137–158, 2006.

[27] A. Gomes and J. Appleton, "Nonlinear cyclic stress-strain relationship of reinforcing bars including buckling," *Eng. Struct.*, vol. 19, no. 10, pp. 822–826, 1997, doi: 10.1016/S0141-0296(97)00166-1.

[28] R. P. Dhakal and K. Maekawa, "Modeling for Postyield Buckling of Reinforcement," *J. Struct. Eng.*, vol. 128, no. 9, pp. 1139–1147, 2002, doi: 10.1061/(asce)0733-9445(2002)128:9(1139).

[29] Chang G. A. and J. B. Mander, "Seismic energy based fatigue damage analysis of bridge columns: Part I - Evaluation of seismic capacity.NCEER Technical Report No. NCEER-94-0006," 1994.

[30] S. H. Megally, P. F. Silva, and F. Seible, "Seismic Response of Sacrificial," *Security*, no. 59, 2002.

[31] A. Shamsabadi and L. Yan, "Closed-F[1] A. Shamsabadi and L. Yan, 'Closed-Form Force-Displacement Backbone Curves for Bridge Abutment-Backfill Systems,' pp. 1–10, 2008, doi: 10.1061/40975(318)159.

[32] P. Wilson and A. Elgamal, "Large-Scale Passive Earth Pressure Load-Displacement Tests and Numerical Simulation," *J. Geotech. Geoenvironmental Eng.*, vol. 136, no. 12, pp. 1634–1643, 2010, doi: 10.1061/(asce)gt.1943-5606.0000386.

[33] J. W. Baker, T. Lin, and S. K. Shahi, "New Ground Motion Selection Procedures and Selected Motions for the PEER Transportation Research Program - DRAFT," *PEER Rep.*, vol. 03, no. March, p. 87, 2011.

[34] L. Jiang, Y. Jiang, Z. Zhang, and A. Usmani, "Thermal Analysis Infrastructure in OpenSees for Fire and its Smart Application Interface Towards Natural Fire Modelling," *Fire Technol.*, vol. 57, no. 6, pp. 2955–2980, 2021, doi: 10.1007/s10694-020-01071-0.

[35] M. Chaboki, M. Heshmati, and A. A. Aghakouchak, "Investigating the behaviour of steel framed-tube and moment-resisting frame systems exposed to fire," *Structures*, vol. 33, no. December 2020, pp. 1802–1818, 2021, doi: 10.1016/j.istruc.2021.05.053.

[36] H. Cilsalar, "Post-earthquake fire collapse performance and residual story drift fragility of two-dimensional structural frames," *Structures*, vol. 38, no. February, pp. 1438–1452, 2022, doi: 10.1016/j.istruc.2022.03.001.

[37] Y. S. Wang, H. Zhou, and J. Y. Wu, "Hybrid fire collapse simulation of reinforced concrete structures under localized fires," *Eng. Struct.*, vol. 292, no. May, p. 116525, 2023, doi: 10.1016/j.engstruct.2023.116525.

[38] *Eurocode 2: Design of concrete structures - Part 1-2: General rules*, vol. 2, no. 2004. 2011.

[39] K. R. Kodur, M. M. S. Dwaikat, and M. B. Dwaikat, "High-temperature properties of concrete for fire resistance modeling of structures," *ACI Mater. J.*, vol. 106, no. 4, p. 390, 2009.

[40] A. Géron, *Hands-on Machine Learning whith Scikit-Learing, Keras and Tensorfow*. 2019.

[41] T. Chen and C. Guestrin, "XGBoost: A scalable tree boosting system," *Proc. ACM SIGKDD Int. Conf. Knowl. Discov. Data Min.*, vol. 13-17-Augu, pp. 785–794, 2016, doi: 10.1145/2939672.2939785.

[42] H. Liu, L. Liu, and H. Zhang, "Boosting feature selection using information metric for classification," *Neurocomputing*, vol. 73, no. 1–3, pp. 295–303, 2009, doi: 10.1016/j.neucom.2009.08.012.

[43] A. Alsahaf, N. Petkov, V. Shenoy, and G. Azzopardi, "A framework for feature selection through boosting," *Expert Syst. Appl.*, vol. 187, no. June 2021, p. 115895, 2022, doi: 10.1016/j.eswa.2021.115895.

[44] Federal Emergency Management Agency (FEMA), "HAZUS-MH MR4 Multi-Hazar d Loss Estimation Methodology – Earthquake Model: Technical Manual. Department of Homeland Security," *Fed. Emerg. Manag. Agency, Washington, …*, pp. 257–261, 2003, [Online]. Available: www.fema.gov/plan/prevent/hazus.